JP&M Engineering
Journal of Petroleum and Mining Engineering

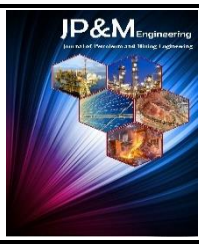

Influence of the Initial Temper Conditions and Post-Deposition Heat Treatments on the Friction Stir Deposition of AA7075.

Yousef G. Y. Elshaghoul [a,b]*, Reham Reda [b] , Sarah A. Elnekhaily [a], Mohamed M. Z. Ahmed [c], Abdou Abdel-Samad [d], Mohamed M. El-Sayed Seleman [a]

[a] Metallurgical and Materials Engineering Dept. Faculty of Petroleum and Mining Engineering, Suez University, Egypt;
[b]Mechanical Engineering Dept. Faculty of Engineering, Suez University, Egypt;
[c]Mechanical Engineering Dept. College of Engineering at Al Kharj, Prince Sattam Bin Abdulaziz University, Al Kharj, Saudi Arabia
[d] Production Engineering and Mechanical Design Dept. Faculty of Engineering, Mansoura University, Mansoura, Egypt,
*Corresponding author e-mail: yousef.gamal@eng.suezuni.edu.eg

Article Info

Received 25 July 2023
Revised 8 August 2023
Accepted 18 August 2023

Keywords

"AA7075-T6; Additive friction stir deposition; Post deposition heat treatment; Microstructure;mechanical properties"

Abstract

Due to the importance of friction stir deposition in many applications such as the repair of surface defects, rib stiffeners, and functional gradient materials for aerospace, biomedical and automotive industries. The present study aims to examine the influence of two different tempered conditions of (T6) and (O) for the as-received material and the post-deposition heat treatment (PDHT) on the mechanical properties and the microstructure of the AA7075 aluminum alloy deposited via additive friction stir deposition technique. To achieve these goals, the FSD experiment was conducted using a 40 mm consumable rod of AA7075-T6 aluminum alloy on a substrate of AA2024-T4 at a constant rotation speed of 400 rev/min and deposition rate of 3 mm/min as a first step to produce continuously multi-layers of AA7075-T6 and AA7075-O. The PDHT was the second step to study the enhancement of the mechanical properties after the deposition process, using two different techniques retrogression re-aging (RRA) and Re-ageing (RA). For the deposited materials the hardness and compression tests as mechanical properties were conducted. In addition, Optical microscopy (OM), scanning electron microscopy (SEM) using an advanced EDS system, and XRD technique were used to analyze the microstructure features. The result showed that after FSD process the hardness of the deposited AA7075-O increased by 25% but the deposited AA7075-T6 attains 90% of the as-received consumable rod. The optimal levels of hardness and compression strength were attained using post-deposition heat treatment of the deposited AA7075-T6 alloy. The resulting average hardness value was measured at 231 HV, while the compressive stress at a strain of 35% was approximately 1142 MPa. The compressive strength of the deposited material was higher than the initial material in both tempered conditions. The microstructure shows a recrystallized grains refinement throughout the deposited AA7075, in which the gain size decreases from 25 µm ± 4 for the as-received material to be 2.06 µm ± 0.51, 1.67 µm ± 0.47 and 4.80 µm ± 1.01 for the DPs AA7075-T6, AA7075-O, and the PDHT, respectively.

Introduction

One potential application for the aerospace industry is to create strong stiffeners and stringer configurations [1]. Aluminium has many advantages, making it a good material. Due to its low price, it is cost-effective. Aluminium's lightweight nature adds to its attraction. It can also be heat treated to get good strength. Heat-treated 2xxx, 6xxx, and 7xxx alloys are quite strong for their weight. Due to inadequate solidification microstructure and porosity, the 2xxx and 7xxx series alloys' fusion zones have lower mechanical characteristics than the as-received material. Thus, these alloys are generally non-weldable [2-4]. So, as a result of low joint strength the fusion welding of these alloys is not appropriate for joining structural components. Recently, for a non-weldable alloy friction-based technology is promising techniques such as friction stir welding (FSW) [4–7], friction stir processing (FSP) [3, 8, 9], and friction stir spot welding (FSSW) [10], friction stir additive manufacturing (FSAM) [11–15], which used for a many purpose such as material joining, surface protection, repairing of defective components, material deposition/surfacing and keyhole refiling.

Nowadays, the Additive friction stir deposition (FSD) technique is used for building (producing) additive manufacturing parts [15-18]. The FSD process begins by rotating a consumable rod material against a substrate while applying an axial downward force. The consumable rod material becomes softer and more plasticized because of the frictional heat generated. The plasticized consumable rod material is deposited onto the substrate. The size of the deposited material is depended on the consumable rod diameter and material properties as well as the

deposition process parameters in terms of rotation speed (RS), axial downward force (F), and deposition feed rate (DR) [19]. Alzahrani et al. [18] studied the applicability of using FSD process to deposit A356 Al Alloy on a substrate of AA 2024 Al alloy at different deposition process parameters. They reported that all the deposition materials tested had harder values than the A356 Al Alloy. Additionally, the greatest harness value of 97.9 HV was applied to the deposition of material at a DR of 3 mm/min and an RS of 1200 rev/min. Ahmed et al. [15] studied the effect of temper conditions on the consumable rod of AA2011 Al alloys during FSD process. The AA2011-O and AA2011-T6 Al alloys had a diameter of 20 mm, and the substrate material was AA5083 Al alloy. They found that the deposited materials of AA2011-O subjected the highest hardness values at the deposition parameters of RS 200 rev/min and DR 1 mm/min compared to the deposited materials of AA2011-T6 and the consumable rod starting materials. Perry et al. [20] studied the microstructure and the crystallographic texture evolutions of the deposited material of AA2024 on a substrate of AA6062 Al alloys. The deposition parameters were 300 rev/min, a linear speed of 120 mm/min, and a feed rate of 0.85 mm/s. They concluded that the AA 2024 deposited materials showed significant grain refining because of continuous dynamic recrystallization.

Post-weld heat treatment (PWHT) is applied to recover the microstructure characteristics of the welds (such as the grains and precipitates) and improve the mechanical properties of the welds [21, 22]. Several studies [23-25] discussed the effect of PWHT on the FSW joints in terms of the microstructure characteristics and mechanical properties. Zhang et al. [25] studied the effect of post-friction stir welding heat treatment at different solution treatments and aging conditions on the microstructure characteristics and the mechanical properties of the AA2195-T8 alloy. They found that the T6 heat treatment condition at 480 °C for 25 min followed by quenching, then aging at 180 °C for 12 h, showed the highest improvement in the joint strength and mechanical properties. Boonma et al. [24] study the influence of PWHT on the impact strength and hardness characteristics of a friction stir welded butt joint made from AA 6061 aluminum alloy. The T6 heat treatment consisted of four distinct conditions, each involving a steady solution heat treatment of 550 °C for 1 h, cold water quenching, and varying periods of aging. The aging condition was 160 °C, 175 °C, 185 °C and 200 °C for 3 h, 9 h and 18 h. They reported that, the applied T6 heat treatment provided a strength recovery of the AA 6061 FSW joints. Aydin et al. [23] discussed the effect of PWHT on the mechanical behaviour of AA 2024-T4 FSW joints. The PWHT condition involved a solution heat treatment at 510 °C for 2.5 h, water quenching, and then either 100 °C or 190 °C for 10 h of aging. The optimum PWHT condition which provided enhancement in the strength and the hardness of the AA2024 FSW joint was solution heat treatment at 510 °C for 2.5 h followed by quenching in water, and aging treatments at 190 °C for 10 h. Pankade et al.[26] study the effect of the PWHT on mechanical properties and corrosion of FSWed AA 7075-T6 aluminum alloy by applying RRA and SDA to the FSW joint, When comparing the tensile strength of AA 7075-T6 before and after FSW, they found a 23% decrease in the latter. After PWHTs, the tensile strength increased by 22% by RRA and 16% by SDA.

The literature study shows that PWHT effectively modifies the microstructure, leading to enhanced mechanical characteristics and corrosion resistance in FSW joints. So far, there has been a lack of studies investigating the effects of initial temper conditions and post-deposition heat treatments on the friction stir deposition of AA7075 onto a substrate of AA2024. These alloys are mostly utilized in aerospace applications, particularly for the production of stiffeners and stringers on a skin. In this study, two distinct temper conditions, namely T6 and O, are employed to subject the deposited AA7075-T6 to heat treatment (HT). Specifically, retrogression re-aging (RRA) and re-aging (RA) techniques are utilized to investigate their effects on the mechanical characteristics and microstructure of the material.

Experimental Work

Starting Material and Methodology

In this context, AA 7075 rods of aluminum alloy with tempered conditions of T6 as BM and (O) after the annealing process are regarded. The rod's diameter used in the FSD processing was 40 mm. Table 1, listed the chemical composition of the as-received material.

Table 1 As-received material chemical composition (wt%).

Elements	wt%
Mg	2.62
Zn	5.72
Cu	1.14
Fe	0.23
Cr	0.20
Mn	0.19
Si	0.36
Al	89.54

(T6 and O) were the two temper conditions that were used to explore how the starting conditions affected the properties of the generated parts. The annealing procedure for the AA7075-T6 as-received sample involved subjecting it to a temperature of 415°C for a duration of 2.5 h. Subsequently, the sample was allowed to cool gradually in a furnace until it reached room temperature, as depicted in Figure 1. To guarantee full fixation throughout the FSD process, as shown in (Figure 2a) the consumable AA7075-T6 and AA7075-O rods were first fixed with the machine shank. Next, the machine was rotated at a constant speed of 400 rev/min while moving downward at a continuous DR of 3 mm/min to reach the substrate plate (Figure 2b). The plastic deformation observed in the rods can be attributed to the generation of frictional heat between the rotating rods and the substrate plate. The application of heat induces the transfer of the material from the rotating rods onto

the substrate plate, leading to the successive creation of several layers as shown in (Figure 2c). To study the PDHT effect on the deposited parts, retrogression re-aging (RRA) and Re-ageing (RA) treatments were applied to the deposited AA7075-T6. The Retrogression and Re-Aging (RRA) treatment consisted of four sequential steps: the (1St) step is solution treatment at a temperature of 480 °C for a duration of 30 minutes, followed by the (2nd) step of rapid cooling in water (quenching). the (3rd) step involved retrogression at a temperature of 180 °C for a soaking period of 0.5 h. Finally, the last stage (4th) step involved re-aging at a temperature of 120 °C for a duration of 24 h. While, the treatment of RA involved a three-step process, which included solution treatment at a temperature of 480 °C for a duration of 2 h, followed by water quenching, and concluding with a re-aging stage at a temperature of 120 °C for a duration of 24 h. The schematic representation of RRA and RA treatments described in (Figure 3a, b) shows all three stages. The process of T6 tempering, which involves aging at a temperature of 120 °C for a duration of 24 h, is generally endorsed and advised [27]. A flow chart, as shown in Figure 4, illustrate the experimental work.

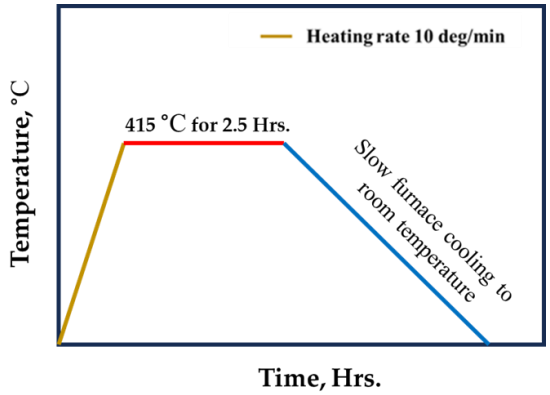

Figure 1 Schematic illustration of annealing heat treatment process for AA7075-T6 to get AA7075-0.

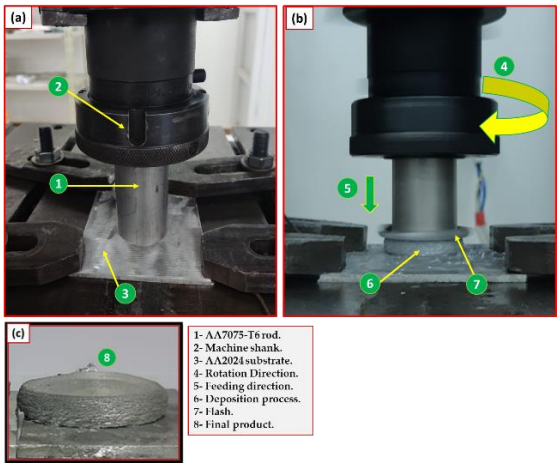

Figure 2 (a) Setup of FSD process of the AA7075 on the AA2024 plate, (b) Onset of the deposition process, (c) Final product.

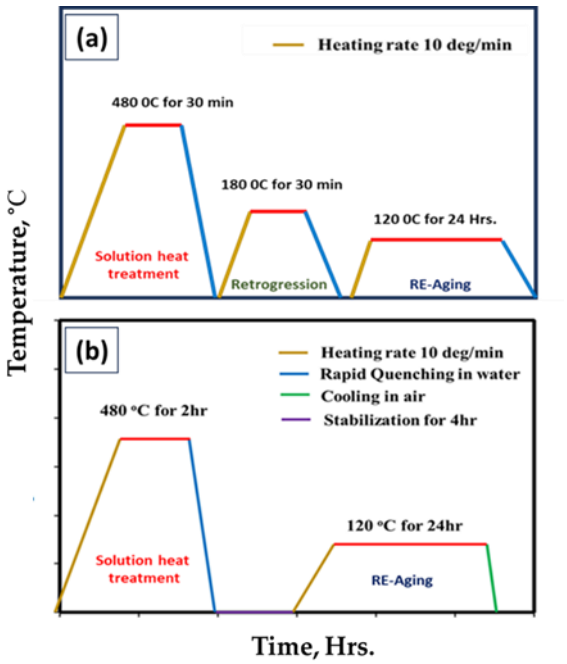

Figure 3 Schematic illustration of the post-heat treatment process (a) for retrogression re-aging (RRA) and, (b) for re-aging (RA).

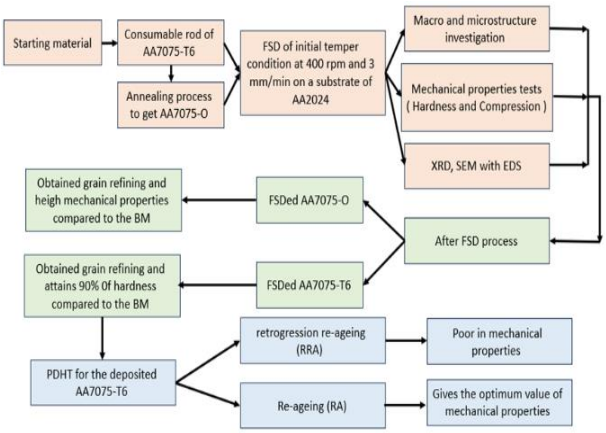

Figure 4 The flowchart of the experimental work.

Characterization of the deposited parts

A standard metallographic procedure was used to prepare the specimens. The samples were milled and polished to an Al2O3 surface finish of 0.05 m, then immersed in (46 mL water, 3 mL HNO3, and 1 HF) Keller's regent solution for chemical etching. To analyse the microstructure, an optical microscope (model BX41M-LED) was used. The grain size distribution and the average grain size are estimated using Image-J Software. A Vickers hardness tester (Model: HWDV-75) was used to measure the material hardness at a 0.5 Kg load and a 15 s dwell period. To plot hardness measurements of the deposited materials in contour maps, the selected area of the tested specimen was divided into four horizontal and fifteen vertical lines with a 2 mm step to adjust the indenter locations, as depicted in Figure 5. The compression test was conducted at room temperature, with the crosshead speed displacement rate held constant at 1 mm/min using a universal testing machine (Model: WDW-300D).

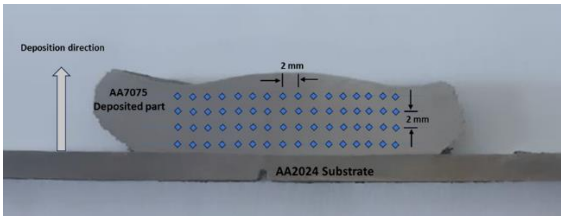

Figure 5 Sketch of the hardness measurements of the AA7075 DPs (L1, L2, L3), near the interface between the DPs and the substrate (L4).

Results and Discussion

Visual inspection and Microstructure of the FSD parts

The study revealed that the FSD process, when applied to the two tempered conditions (T6 and O), resulted in the formation of multiple layers characterized by a lack of flaws and strong adhesion between the deposited layers and the substrate material. Figure 6a, and c represents the deposited part and the cross-section of the product for the deposited AA7075-T6, respectively. While Figure 5b, d is for the deposited AA7075-O.

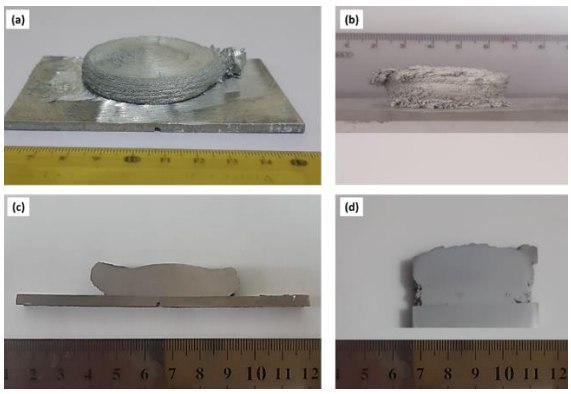

Figure 6 The visual and macrostructure of (a) the deposited AA7075-T6, (b) the deposited AA7075-O, (c) the cross-section of the AA7075-T6 product, and (d) the cross-section of the AA7075-O product.

Figure 7, illustrates the optical micrographs of AA7075-T6 as received material, deposited layers of AA7075-T6, deposited layers of AA7075-O and post-deposition heat-treated AA7075-T6 (PDHT) conditions. The grains of the as-received material are oriented along the direction of rolling, as shown in (Figure 7a). (Figure 7b, c) depicts the tiny equiaxed grains structure that results from dynamic recrystallization during the deposition process. A grain growth due to the post-heat treatment process was detected as shown in (Figure 7d). The average grain size (Figures 8a, b, and c) of the deposited AA7075-T6, deposited AA7075-O, and the PDHT were calculated as 2.06 µm ± 0.51, 1.67 µm ± 0.47 and 4.80 µm ± 1.01 respectively.

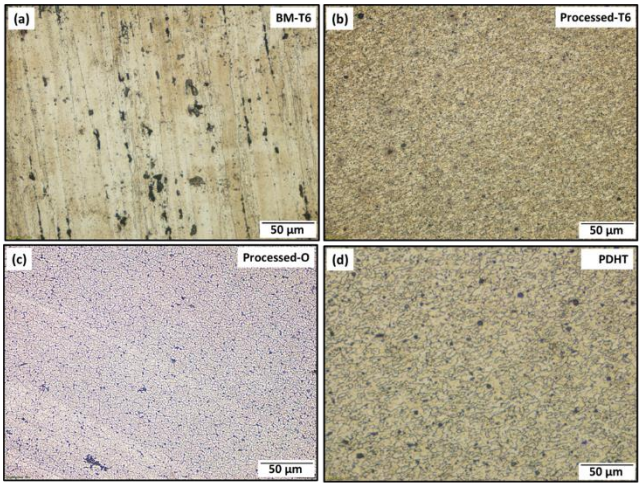

Figure 7 The microstructure of, (a) AA7075-T6 as-received material, (b) deposited AA7075-T6 (c) deposited AA7075-O, and (d) after the PDHT process.

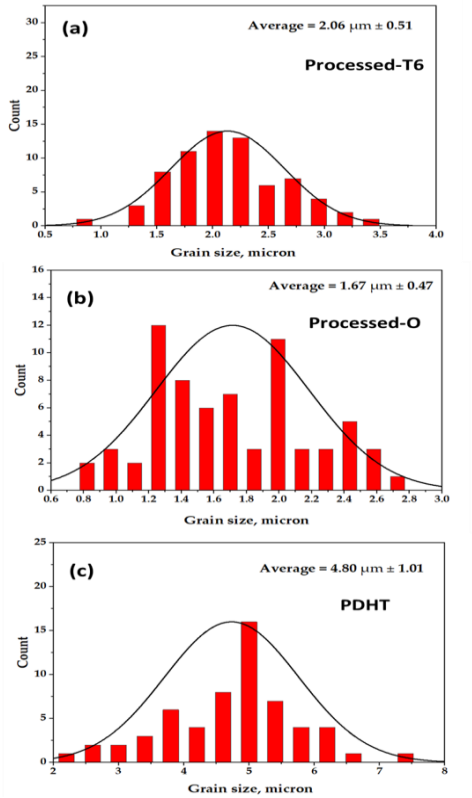

Figure 8 Grain size analysis of, (a) AA7075-T6 as-received material, (b) after the FSD process, and (c) after the PDHT process.

Mechanical properties Hardness and Compression

The hardness value is a reliable predictor of the mechanical properties of the material, and its value is influenced by the deformation process variables, the heat treatment regimen, and the chemical composition of the BM. Figure (9a, b, c, and d) shows the hardness maps obtained from hardness measurements of the initial AA7075-O and AA7075-T6 materials and their deposited parts produced at DR of 3 mm/min and RS of 400 rev/min. The hardness value of the deposited AA7075-T6 was 165 HV which` attains about 90% of the AA7075-T6 base metal of 185 HV. While in the case of AA7075-O, the hardness value of the deposited part was 116 HV which was an

 DOI: 10.21608/jpme.2023.224934.1170

increase of 28% than the AA7075-T6 BM of 90 HV. Due to the decrease in hardness value for the deposited AA7075-T6, the PDHTs were applied for the deposited AA7075-T6 and the hardness value found a noticeable improvement compared to those of BM and the deposited AA7075-T6 where the value of hardness was 231 HV in case of the heat treatment regimen (RA). But on the contrary, in the case of (RRA) regimen, the hardness value of the deposited AA7075-T6 decreased to 120 HV. It can be noted that from the hardness maps a homogeneous uniform distribution of hardness value due to the additive friction stir deposition process. Therefore, it can be reasonably assumed that in AA7075-O the grain refining leads to the improvement but in the case of AA7075-T6 the intermetallics have a more profound influence on the hardness of the material than the grain size and that will be discussed later. The compression test is of utmost importance in assessing the response of the tested materials to compressive forces. Figure 10 illustrates the stress-strain compression curves at a strain of 35% for the starting materials in two tempered conditions, as well as the deposited parts. The compressive strength of the deposited material surpasses that of the original material in both tempered states. As shown in Figure 11, the optimum hardness and compression strength were achieved with post-deposition heat treatment of the deposited AA7075-T6, where the average hardness value was 231 HV and compressive stress at 35% strain was about 1142MPa, respectively.

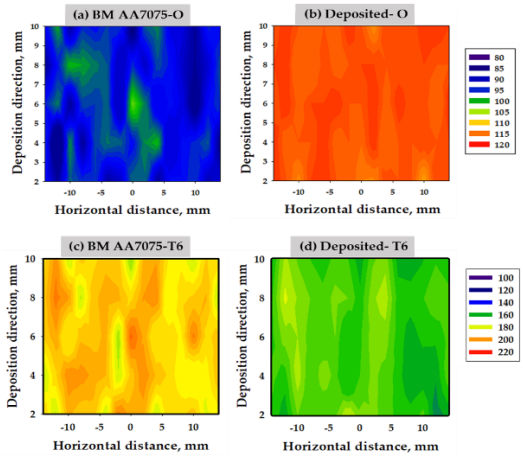

Figure 9 The hardness maps of, (a) aa7075-O as-received material, (b) deposited AA7075-O (c) AA7075-T6 as-received material, and (d) deposited AA7075-T6.

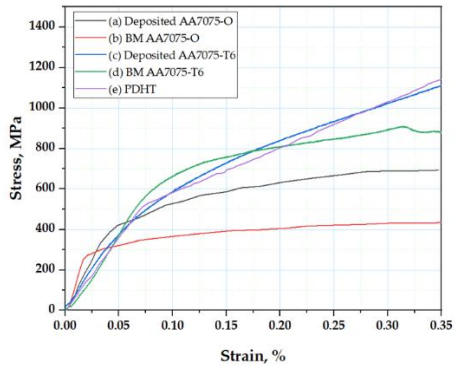

Figure 10 The compressive stress strain curves of, (a) AA7075-O as-received material, (b) deposited AA7075-O (c) AA7075-T6 as-received material, and (d) deposited AA7075-T6.

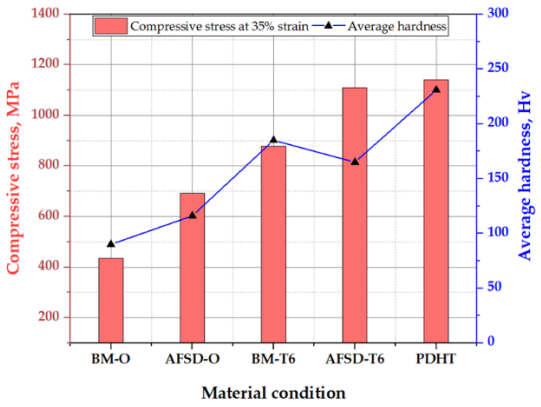

Figure 11 The conclusion of the mechanical properties in terms of hardness and compression for all material conditions.

XRD and SEM with EDS Analysis

The XRD examination is used to detect the intermetallic effect on the mechanical properties of the AA7075-T6. As shown in (Figure 12b) it was illustrated that a clear appearance of MgZn2 phase peaks at 2-theta of 40.485, 41.337 with FWHM of 0.27 and 0.31, respectively, due to the sufficient heat generation during FSD process and the gradually cooling in the air after FSD process allows the size and the distribution of precipitated phase have a difference between the BM and deposition zone. So, the precipitated phase may be the main factor affecting the hardness of the deposited parts. The size of the precipitated $MgZn_2$ phase increases in the DP zone, after the formation of these precipitate particles, the material's microstructure will soften, which will have a negative impact on the hardness value of the deposited part of the T6 tempered condition [28]. This can be addressed by rapid cooling and an appropriate heat treatment process [29]. On the other side as shown in (Figure 12c) the XRD graph illustrates that the η phase was not observed due to the appropriate aging mechanism of rapid quenching in water an aging temperature of 120 °C and an aging time of 2 h. Suleyman et al. [28] study the effect of aging temperature and duration time on the precipitate behaviour of AA7075 aluminum alloy According to these findings, $MgZn_2$ precipitation is not seen at aging temperatures between 120 and 160 °C. After the creation of $MgZn_2$ precipitates, the microstructure will become more pliable if the aging process is continued for a longer period or at a higher temperature.

To confirm the potential presence of intermetallic compounds within the AA7075-T6 rod's microstructure, the deposited material, and after the post-deposited heat treatment material further investigation is required so that an advanced scanning electron microscopy (SEM) with EDS analysis system was used as shown in Figure 13. The EDS analysis as shown in Figure 13 a, b revealed the presence of three

distinct intermetallic compounds inside the aluminum matrix. Specifically, Spot 1 exhibited a rod-like structure consisting of $MgZn_2$, Spot 2 had an almost-spherical morphology composed of AlCuMg, while Spot 3 exhibited an uneven shape containing Al_7Cu_2Fe. The EDS spots 1, 2, and 3 are represented in Figure 13 d, e, and f respectively. These intermetallics differ in morphology and phase composition. The determination of intermetallic morphologies inside the aluminum matrix alloy is influenced by various factors, including chemical composition, alloying element type, processing methodology, and heat treatment regimen [29], [30].

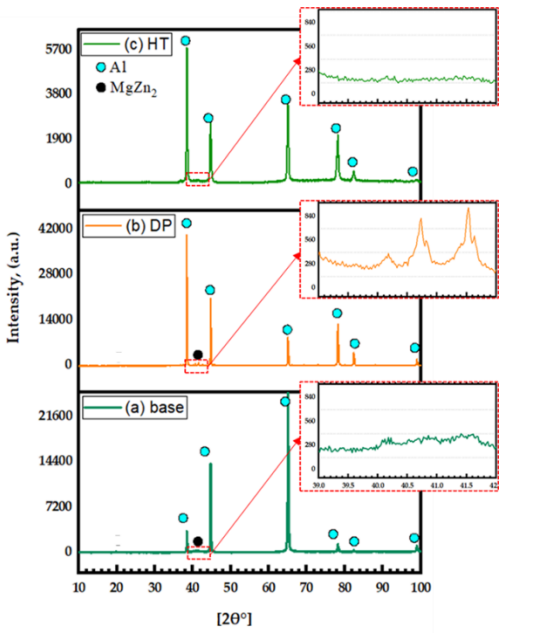

Figure 12 XRD analysis of, (a) AA7075-T6 as-received material, (b) after the FSD process, and (c) after the PDHT process.

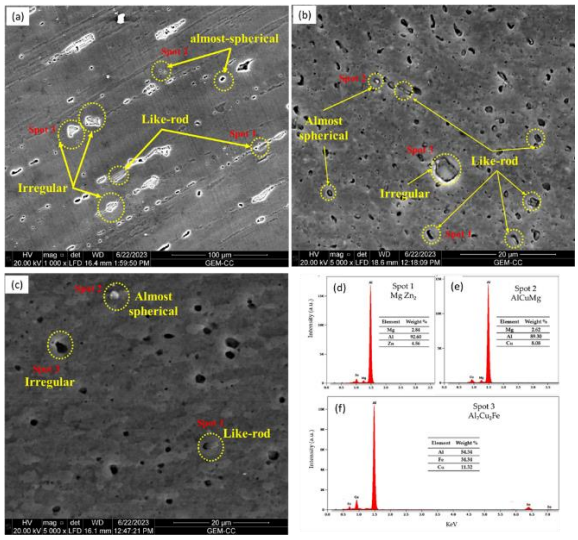

Figure 13 SEM-images show microstructures of (a) AA7075-T6 rod BM, (b) DP processed at 400 rev/min and 3 mm/min, (c) PDHT deposited AA7075-T6 (d) EDS spot 1 (e) EDS spot 2 and (f) EDS spot 3.

Conclusions

- The suggested additive friction stir deposition technique successfully produced a continuous multi-layer of AA7075-T6 and AA7075-O on a substrate of AA2024 as stiffeners on the skin.
- The mechanical properties of AA7075-O increase after the FSD process. Where the hardness value increased by 28% than the BM and the compressive strength improved compared to the as-received material.
- The hardness of the deposited AA7075-T6 decreased by 10% after the FSD process to the BM and the compressive strength improved by 26% compared to the as-received material.
- Applying the post-deposition heat treatment to the deposited AA7075-T6 improve the hardness value compared to the BM and the deposited part.
- In AA7075-T6 the intermetallics have a more profound influence on the hardness of the material than the grain size.
- The deposition process and the PDHT affect the size and dispersion of intermetallics ($MgZn_2$, AlCuMg, and Al_7Cu_2Fe), and these precipitates have a direct impact on the strengthening of the deposited layers.
- The subsequent phase of this study entails the application of the effective PDHT procedure on items produced under the :O" tempered state, followed by the commencement of preliminary experiments for the production of a linear surface deposition.

Funding sources

This research received no external funding.

Conflicts of interest

There are no conflicts to declare.

Acknowledgements

The authors extend their appreciation to the Suez and Sinai Metallurgical and Materials Research Center of Scientific Excellence (SSMMR-CSE).

References

[1] S. M. Puleo, "Additive Friction Stir Manufacturing of 7055 Aluminum Alloy," 2016. [Online]. Available: https://scholarworks.uno.edu/honors_theses/75

[2] M. Yunus and T. Alamro, "Evaluation of wear and corrosion properties of FSWed aluminum alloy plates of AA2020-T4 with heat treatment under different aging periods," Reviews on Advanced Materials Science, vol. 61, no. 1, pp. 687–697, Jan. 2022, doi: 10.1515/rams-2022-0261.

[3] R. S. Mishra and Z. Y. Ma, "Friction stir welding and processing," Materials Science and Engineering R: Reports, vol. 50, no. 1–2. Aug. 31, 2005. doi: 10.1016/j.mser.2005.07.001.

[4] M. M. Z. Ahmed, El-Sayed Seleman, M.M., Z. A. Zidan, R. M. Ramadan, S. Ataya, and N. A. Alsaleh, "Microstructure and mechanical properties of dissimilar friction stir welded AA2024-T4/AA7075-T6 T-butt joints,"

Metals (Basel), vol. 11, no. 1, pp. 1–19, Jan. 2021, doi: 10.3390/met11010128.

[5] C. Zhang, G. Huang, Y. Cao, Y. Zhu, and Q. Liu, "On the microstructure and mechanical properties of similar and dissimilar AA7075 and AA2024 friction stir welding joints: Effect of rotational speed," J Manuf Process, vol. 37, pp. 470–487, Jan. 2019, doi: 10.1016/j.jmapro.2018.12.014.

[6] A. M. Sadoun, A. Wagih, A. Fathy, and A. R. S. Essa, "Effect of tool pin side area ratio on temperature distribution in friction stir welding," Results Phys, vol. 15, Dec. 2019, doi: 10.1016/j.rinp.2019.102814.

[7] A. M. Sadoun, A. F. Meselhy, and A. W. Deabs, "Improved strength and ductility of friction stir tailor-welded blanks of base metal AA2024 reinforced with interlayer strip of AA7075," Results Phys, vol. 16, Mar. 2020, doi: 10.1016/j.rinp.2019.102911.

[8] M. M. Z. Ahmed, El-Sayed Seleman, M.M., R. G. Eid, I. Albaijan, and K. Touileb, "The Influence of Tool Pin Geometry and Speed on the Mechanical Properties of the Bobbin Tool Friction Stir Processed AA1050," Materials, vol. 15, no. 13, Jul. 2022, doi: 10.3390/ma15134684.

[9] I. Albaijan, M. M. Z. Ahmed, El-Sayed Seleman, M.M., K. Touileb, M. I. A. Habba, and R. A. Fouad, "Optimization of Bobbin Tool Friction Stir Processing Parameters of AA1050 Using Response Surface Methodology," Materials, vol. 15, no. 19, Oct. 2022, doi: 10.3390/ma15196886.

[10] M. M. Z. Ahmed, El-Sayed Seleman, M.M., E. Ahmed, H. A. Reyad, N. A. Alsaleh, and I. Albaijan, "A Novel Friction Stir Deposition Technique to Refill Keyhole of Friction Stir Spot Welded AA6082-T6 Dissimilar Joints of Different Sheet Thicknesses," Materials, vol. 15, no. 19, Oct. 2022, doi: 10.3390/ma15196799.

[11] El-Sayed Seleman, M.M.; Ataya, S.; Ahmed, M.M.Z.; Hassan, A.M.M.; Latief, F.H.; Hajlaoui, K.; El-Nikhaily, A.E.; Habba, M.I.A. The Additive Manufacturing of Aluminum Matrix Nano Al2O3 Composites Produced via Friction Stir Deposition Using Different Initial Material Conditions. Materials 2022, 15, doi:10.3390/ma15082926.

[12] R. Joey Griffiths, D. T. Petersen, D. Garcia, and H. Z. Yu, "Additive friction stir-enabled solid-state additive manufacturing for the repair of 7075 aluminum alloy," Applied Sciences (Switzerland), vol. 9, no. 17, Sep. 2019, doi: 10.3390/app9173486.

[13] F. Khodabakhshi and A. P. Gerlich, "Potentials and strategies of solid-state additive friction-stir manufacturing technology: A critical review," Journal of Manufacturing Processes, vol. 36. Elsevier Ltd, pp. 77–92, Dec. 01, 2018. doi: 10.1016/j.jmapro.2018.09.030.

[14] E. Elfishawy, M. M. Z. Ahmed, and El-Sayed Seleman, M.M., "Additive Manufacturing of Aluminum Using Friction Stir Deposition," in Minerals, Metals and Materials Series, Springer, 2020, pp. 227–238. doi: 10.1007/978-3-030-36296-6_21.

[15] M. M. Z. Ahmed, El-Sayed Seleman, M.M., E. Elfishawy, B. Alzahrani, K. Touileb, and M. I. A. Habba, "The effect of temper condition and feeding speed on the additive manufacturing of AA2011 parts using friction stir deposition," Materials, vol. 14, no. 21, Nov. 2021, doi: 10.3390/ma14216396.

[16] M. Srivastava, S. Rathee, S. Maheshwari, A. Noor Siddiquee, and T. K. Kundra, "A Review on Recent Progress in Solid State Friction Based Metal Additive Manufacturing: Friction Stir Additive Techniques," Critical Reviews in Solid State and Materials Sciences, vol. 44, no. 5. Taylor and Francis Inc., pp. 345–377, Sep. 03, 2019. doi: 10.1080/10408436.2018.1490250.

[17] A. Kumar Srivastava, N. Kumar, and A. Rai Dixit, "Friction stir additive manufacturing – An innovative tool to enhance mechanical and microstructural properties," Materials Science and Engineering B: Solid-State Materials for Advanced Technology, vol. 263. Elsevier Ltd, Jan. 01, 2021. doi: 10.1016/j.mseb.2020.114832.

[18] Alzahrani, B.; El-Sayed Seleman, M.M.; Ahmed, M.M.Z.; Elfishawy, E.; Ahmed, A.M.Z.; Touileb, K.; Jouini, N.; Habba, M.I.A "The applicability of die cast a356 alloy to additive friction stir deposition at various feeding speeds," Materials, vol. 14, no. 20, Oct. 2021, doi: 10.3390/ma14206018.

[19] J. J. S. Dilip and G. D. Janaki Ram, "Microstructure evolution in aluminum alloy AA 2014 during multi-layer friction deposition," Mater Charact, vol. 86, pp. 146–151, 2013, doi: 10.1016/j.matchar.2013.10.009.

[20] M. E. J. Perry, R. J. Griffiths, D. Garcia, J. M. Sietins, Y. Zhu, and H. Z. Yu, "Morphological and microstructural investigation of the non-planar interface formed in solid-state metal additive manufacturing by additive friction stir deposition," Addit Manuf, vol. 35, Oct. 2020, doi: 10.1016/j.addma.2020.101293.

[21] S. K. Nirgude, C. M. Choudhari, and S. D. Kalpande, "A Review on Pre/Post Treatments Used in Friction Stir Welding." [Online]. Available: https://ssrn.com/abstract=3101621

[22] Q. Qiao, Y. Su, H. Cao, D. Zhang, and Q. Ouyang, "Effect of post-weld heat treatment on double-sided friction stir welded joint of 120 mm ultra-thick SiCp/Al composite plates," Mater Charact, vol. 169, Nov. 2020, doi: 10.1016/j.matchar.2020.110668.

[23] H. Aydin, A. Bayram, and I. Durgun, "The effect of post-weld heat treatment on the mechanical properties of 2024-T4 friction stir-welded joints," Mater Des, vol. 31, no. 5, pp. 2568–2577, May 2010, doi: 10.1016/j.matdes.2009.11.030.

[24] J. Boonma, S. Khammuangsa, K. Uttarasak, J. Dutchaneephet, C. Boonruang, and N. Sirikulrat, "Post-weld heat treatment effects on hardness and impact strength of aluminum alloy 6061 friction stir Butt weld," Mater Trans, vol. 56, no. 7, pp. 1072–1076, 2015, doi: 10.2320/matertrans.M2015074.

[25] J. Zhang, X. S. Feng, J. S. Gao, H. Huang, Z. Q. Ma, and L. J. Guo, "Effects of welding parameters and post-heat treatment on mechanical properties of friction stir welded AA2195-T8 Al-Li alloy," J Mater Sci Technol, vol. 34, no. 1, pp. 219–227, Jan. 2018, doi: 10.1016/j.jmst.2017.11.033.

[26] S. B. Pankade, P. M. Ambad, R. Wahane, and C. L. Gogte, "Effect of the Post-weld Heat Treatments on Mechanical and Corrosion Properties of Friction Stir-Welded AA 7075-T6 Aluminium Alloy," 2019, pp. 79–94. doi: 10.1007/978-981-13-0378-4_4.

[27] H. Y. Hunsicker, "Rosenhain Centenary Conference: The Contribution of Physical Metallurgy to Engineering Practice," 1976.

[28] S. Kilic, I. Kacar, M. Sahin, F. Ozturk, and O. Erdem, "Effects of aging temperature, time, and pre-strain on mechanical properties of AA7075," Materials Research, vol. 22, no. 5, 2019, doi: 10.1590/1980-5373-MR-2019-0006.

[29] A. D. Isadare, B. Aremo, M. O. Adeoye, O. J. Olawale, and M. D. Shittu, “Effect of heat treatment on some mechanical properties of 7075 Aluminium alloy,” Materials Research, vol. 16, no. 1, pp. 190–194, Jan. 2013, doi: 10.1590/S1516-14392012005000167.

[30] Z. Hao, D. Shaokang, M. Zeming, and W. Jun, “Study on the precipitation behavior of precipitates of 7075 aluminum alloy friction stir welding joint,” in Materials Science Forum, Trans Tech Publications Ltd, 2020, pp. 37–46. doi: 10.4028/www.scientific.net/MSF.1003.37.